Individual- versus group-optimality in the production of secreted bacterial compounds

Konstanze T. Schiessl[1,2,†] , Adin Ross-Gillespie[3], Daniel M. Cornforth[4], Michael Weigert[3], Colette Bigosch[5], Sam P. Brown[4], Martin Ackermann[1,2,*], Rolf Kümmerli[3, 6*]

* contributed equally
[†] Current address: Department of Biological Sciences, Columbia University, 1212 Amsterdam Avenue, New York, NY 10027, USA.

1 Department of Environmental Microbiology, Swiss Federal Institute of Aquatic Science and Technology (Eawag), Überlandstrasse 133, 8600 Dübendorf, Switzerland.

2 Department of Environmental Systems Science, Swiss Federal Institute of Technology (ETH Zurich), Universitätsstrasse 16, 8092 Zürich, Switzerland.

3 Department of Plant and Microbial Biology, University of Zürich, Winterthurerstrasse 190, 8057 Zürich, Switzerland.

4 School of Biological Sciences, Georgia Institute of Technology, Atlanta, USA.

5 Department of Health Sciences and Technology, Swiss Federal Institute of Technology (ETH Zurich), Universitätsstrasse 2, 8092 Zürich, Switzerland.

6 Department of Quantitative Biomedicine, University of Zürich, Winterthurerstrasse 190, 8057 Zürich, Switzerland.

Correspondence should be addressed to: konstanze.schiessl@gmail.com
Department of Biological Sciences, Columbia University, 1212 Amsterdam Avenue, New York, NY 10027, USA.

Running head: Optimal production of secreted bacterial compounds

Keywords: division of labor**,** bacteria**,** group level selection, siderophores, optimal production, economy of scales

Abstract

How unicellular organisms optimize the production of compounds is a fundamental biological question. While it is typically thought that production is optimized at the individual-cell level, secreted compounds could also allow for optimization at the group level, leading to a division of labor where a subset of cells produces and shares the compound with everyone. Using mathematical modelling, we show that the evolution of such division of labor depends on the cost function of compound production. Specifically, for any trait with saturating benefits, linear costs promote the evolution of uniform production levels across cells. Conversely, production costs that diminish with higher output levels favor the evolution of specialization – especially when compound shareability is high. When experimentally testing these predictions with pyoverdine, a secreted iron-scavenging compound produced by *Pseudomonas aeruginosa*, we found linear costs and, consistent with our model, detected uniform pyoverdine production levels across cells. We conclude that for shared compounds with saturating benefits, the evolution of division of labor is facilitated by a diminishing cost function. More generally, we note that shifts in the level of selection from individuals to groups do not solely require cooperation, but critically depend on mechanistic factors, including the distribution of compound synthesis costs.

Introduction

The production of proteins and metabolites is at the basis of many cellular processes. Because of its fundamental importance, there has been much interest in understanding the mechanisms that control compound production at the cellular level (Dekel and Alon 2005; Shachrai et al. 2010; Eames and Kortemme 2012; Price et al. 2013). The general consensus is that there should be a production optimum, at which the net benefit of producing a specific compound (protein or metabolite) peaks. Moving away from that optimum either results in wasteful overproduction or insufficient compound supply. Indeed, experimental work has demonstrated that populations of unicellular organisms evolve towards such optima in laboratory settings (Dekel and Alon 2005; Poelwijk et al. 2011).

One implicit assumption of the above-mentioned work on unicellular organisms is that optimality is achieved at the level of the individual. This means that every individual in a population is expected to tune its compound expression level to the same optimum. However, bacteria and other microbes are not solitary organisms, but often live in dense social groups, where they can interact and communicate with one another (West et al. 2007; Asfahl and Schuster 2017; Özkaya et al. 2017). This opens the possibility for optimality in compound production to arise at the level of the clonal group and not the individual. Indeed, recent experimental studies report cases of bimodal trait expression patterns

41 across individuals in clonal groups, which could reflect group-level optimization
42 (Diard et al. 2013; van Gestel et al. 2015).
43
44 Here, we formally ask whether group optimality in compound production in a
45 clonal group is indeed possible and examine the conditions for which
46 heterogenous suboptimal individual behavior can promote optimality at the level
47 of the group (i.e. representing a case where clonal groups become a functional
48 unit; (Ackermann 2015). (Frank 2013) proposed that heterogeneous expression
49 profiles could be particularly common for secreted extra-cellular compounds. The
50 reasoning is that secreted compounds, including enzymes and secondary
51 metabolites, can be shared at the level of the clonal group, thereby decoupling
52 individual expression levels from fitness returns. In other words, the benefit an
53 individual gains from the production of a shared compound is determined not by
54 the individual's own investment, but by the production level of the entire group
55 (Frank 2013). High shareability could thus potentially trigger the evolution of a
56 group-optimal strategy, characterized by a type of division of labor where the
57 clonal group splits into phenotypic producers and non-producers. This split could
58 be mechanistically implemented either by intrinsic or extrinsic (signal-induced)
59 bistable expression of the relevant synthesis genes (Dubnau and Losick 2006;
60 Veening et al. 2008; Ackermann et al. 2008; West and Cooper 2016), combined
61 with phenotypic switching promoting a stable proportion of producers and non-
62 producers in the population (Julou et al. 2013; Diard et al. 2013).

63

64 Apart from the aspect of shareability, we further hypothesize that whether or not
65 a shift from individual to group level optimization occurs also depends on the
66 underlying cost and benefit functions of a compound. Previously published data
67 show biological examples of costs that increase either linearly or exponentially
68 with the amount of compound produced (Dekel and Alon 2005; Shachrai et al.
69 2010; Eames and Kortemme 2012; Price et al. 2013). In the case of a linear cost
70 function, we predict that group-level optimization should not evolve because
71 costs are additive, thus providing no fitness incentives for cells to engage in
72 specialization. Conversely, diminishing cost functions should be more conducive
73 for group-level optimization because the principle of the economies of scale
74 apply – the cost per compound decreases with higher production levels (Case et
75 al. 2011).

76

77 We mathematically formalized these hypotheses to define the conditions required
78 for group-level optimization to evolve. We then empirically tested our hypotheses
79 in a bacterial model system. Specifically, we used the production of pyoverdine, a
80 siderophore synthesized via nonribosomal peptide synthetases, which is
81 secreted by the bacterium *Pseudomonas aeruginosa* to scavenge iron from the
82 environment (Visca et al. 2007). Pyoverdine production has become a model trait
83 to study social interactions in bacteria, and multiple studies have shown that this
84 compound can be shared between cells that possess the specific receptor

85 required for pyoverdine uptake (e.g. (Griffin et al. 2004; Cordero et al. 2012;
86 Inglis et al. 2016). However, the level of shareability for this and other
87 compounds depends on a number of factors, including the diffusivity of the
88 environment and cell density (Ross-Gillespie et al. 2009; Kümmerli et al. 2009a;
89 Weigert and Kümmerli 2017). This means that the level to which pyoverdine can
90 be shared as a public good among cells might vary in the environment and that is
91 why we included shareability as a key parameter in our model.
92
93 Pyoverdine, like many other secreted secondary metabolites (e.g. antibiotics,
94 toxins, surfactants, siderophores), is produced via nonribosomal peptide
95 synthesis (NRPS) instead of ribosomal synthesis (Caboche et al. 2007; Miethke
96 and Marahiel 2007). Nonribosomal peptide synthesis requires the buildup of
97 complex synthesis machineries prior to metabolite production (at least 23
98 proteins in the case of pyoverdine; (Visca et al. 2007; Schalk and Guillon 2013).
99 Given this mechanistic background, we postulate that if the cost of building up
100 this dedicated cellular machinery is substantial compared to the production of the
101 compound itself then the system should be characterized by a diminishing cost
102 function. Conversely, if the majority of pyoverdine cost is attributable to molecule
103 synthesis and not to the buildup of the biosynthetic machinery then the system
104 should be characterized by a linear cost function. To test these predictions, we
105 measured cost and benefit functions of pyoverdine production using an
106 engineered *P. aeruginosa* strain, where pyoverdine synthesis can be gradually

induced. Subsequently, we combined automated flow cytometry with single-cell microscopy to examine whether all individual cells within a clonal group show uniform pyoverdine production levels or whether specialization occurs. These analyses allow us to examine whether *P. aeruginosa* has been exposed to selection for optimal production at the group level in the evolutionary past, in its natural environment.

Material and Methods

Mathematical model

We used a simple mathematical model to explore how cost and benefit functions interact to shape bacterial fitness in a clonal group where individuals either all produce the same amount of compound (e.g. pyoverdine) or engage in specialization where only a fraction produces the compound. We can express the net benefit β to a bacterial group as

$$ß(x, p, s) = p[B(sxp + (1 - s)x) - C(x)] + (1 - p)[B(sxp)] \quad (1)$$

where B is a function representing the gross benefit of the compound, and C is the absolute cost of compound production. p is the proportion of producers in the group, producing a quantity x (the other individuals produce none), and s is the

129 shareability parameter, describing the proportion of compound that is shared
130 among clonemates. Our model focuses on a complete division of labor where
131 production phenotypes are distributed in a binary on-off way. We chose this
132 extreme setup for two reasons. First, biological examples of phenotypic division
133 of labor include such binary switches (Ackermann et al. 2008; Diard et al. 2013;
134 van Gestel et al. 2015). Second, although other scenarios of division of labor
135 (e.g. where cells produce either low or high amounts of a compound) would also
136 be realistic, we expect highest net group benefits for the on-off case. This is
137 because with less extreme forms of specialization all cells would still experience
138 some level of production costs, which would compromise the net benefits gained
139 by specialization. We further assume that an individual's production state
140 (producer vs. non-producer) is non-heritable, and that individuals can change
141 their state at any moment in time (see (Julou et al. 2013) for an empirical
142 analysis of state switching). We note that the ability to switch production state is
143 an important prerequisite for the evolution of phenotypic division of labor in a
144 clonal group, as it guarantees a stable proportion of producers in the population.
145
146 The first term in the equation represents the fitness of a cell engaging in
147 production of the secreted compound. The benefit experienced by a producer cell
148 is a function of the amount of compound it can access, which is determined by
149 the products released and shared by others (sxp) as well as those released by
150 itself but not shared with others $(1-s)x$. Producers also pay a cost for production,

151 which is a function of their production (x). The second term describes the fitness
152 of a non-producer, which equals the benefits obtained from others' secretions.
153
154 We considered two monotonically increasing absolute cost functions: a
155 diminishing cost function captured by $C(x) = g(1\text{-}e^{-hx})$, and a linear cost function
156 captured by $C(x) = k(x)$, where g, h, and k are scaling factors (Figure 1A, B).
157 Note that we use an arbitrary diminishing cost function for our main analysis, but
158 provide a general mathematical proof that shows that our findings hold for any
159 type of diminishing cost function (see Supplemental Information). For the gross
160 benefit function, we assume saturating returns with higher compound availability,
161 captured by $B(x) = d(1\text{-}e^{-fx})$ with d and f as scaling factors (Figure 1A+B).
162 Saturating returns are common for secreted metabolites (Foster 2004; Cornforth
163 et al. 2012).
164
165 ***Strains***
166 All our experiments were carried out with the clinical isolate *P. aeruginosa* PAO1
167 (ATCC 15692), the most widely studied strain of this species. To measure costs
168 and benefits of pyoverdine production, we constructed the conditional pyoverdine
169 mutant PAO1-*pvdSi*, where we put the production of pyoverdine under the
170 control of the IPTG inducible promoter P_{tac}. Specifically, we replaced the native
171 promoter of *pvdS*, the gene coding for the iron starvation sigma factor PvdS,
172 which controls the expression of genes coding for enzymes involved in

173 nonribosomal peptide synthesis of siderophores. We PCR-amplified the flanking
174 regions (FR1 upstream: 836 bp; and FR2 downstream: 987 bp) of the native
175 *pvdS* promoter using the following set of primers (FR1F: 5'- ggg ata cac cgg aga
176 gga ata -3', FR1R: 5' - ttt gcc att ctc acc gga ttt gat gga ggg gag aaa ttc tt -3' /
177 FR2F-*SacI*: 5' - gcg cga gct cat gtc gga aca act gtc tac ccg -3', FR2R-*KpnI*: 5' –
178 gcg cgg tac cat cca tat gcc cgc tgc gac a - 3'). FR2 features two restriction sites
179 (*SacI* and *KpnI*), which we used to clone this fragment into the pME6032 vector
180 featuring the P_{tac} promoter and *lacI* (repressor of P_{tac}). We then PCR-amplified
181 the *lacI* - P_{tac} - FR2 construct using the primers ampF (5'- aat ccg gtg aga atg gca
182 aa -3') and ampR (5'- tcc gag gcc tcg aga tct at -3'), and subsequently carried out
183 fusion PCR with this amplicon and FR1, which features a 20 bp overhang (see
184 FR1R) reverse complementary to the *lacI* sequence. Fusion PCR included a first
185 set of cycles, where the *lacI* - P_{tac} - FR2 amplicon and FR1 could hybridize via
186 the overhang in the absence of primers, and therefore mutually serve each other
187 as template and primer. During a second set of cycles, the final construct of 3242
188 bp length was amplified using the primers FR1 and ampR. This fragment was
189 ligated into pGEM-T easy (A1360, Promega) for storage, and cloned into
190 pME3087, a suicide vector, which we transformed into the *Escherichia coli* S17-1
191 donor strain. We then carried out mating between the S17-1 donor and the PAO1
192 recipient. Single crossovers were selected on LB agar supplemented with
193 tetracycline (100 μg/ml to select against wildtype PAO1) and chloramphenicol (10
194 μg/ml to select against S17-1). We grew one single crossover colony overnight in

195 LB at 37°C, during which double crossovers can occur (either reverting back to
196 wildtype or replacing the native *pvdS* promoter with our inducible construct). To
197 enrich for double crossovers, we added tetracycline (20 *µ*g/ml, a bacteriostatic
198 concentration at which non-tetracycline resistant strains stop growing).
199 Subsequently, we added carbenicillin (2000 *µ*g/ml) to selectively kill the growing
200 tetracycline-resistant single crossovers. After cell washing and plating, we picked
201 ~100 colonies from LB plates and screened for conditional pyoverdine mutants,
202 using IPTG-induction assays and sequencing of the *pvdS* promoter site.
203
204 To investigate heterogeneity in pyoverdine expression, we used PAO1*pvdA-gfp*,
205 a transcriptional reporter (chromosomal insertion: *att*B::*pvdA-gfp*), which links
206 transcription of *egfp* to the transcription of *pvdA*, one of the pyoverdine
207 biosynthesis genes (Kaneko et al. 2007). As negative control (i.e. no GFP
208 expression), we used the wildtype PAO1 strain obtained from Pierre Cornelis'
209 laboratory (Ghysels et al. 2004). As positive control, we used a constitutive GFP-
210 expressing derivate of PAO1 (PAO1-*gfp*, chromosomal insertion: *att*Tn7:: P_{tac} -
211 *gfp*) (Lambertsen et al. 2004). Finally, we generated the double-reporter strain
212 PAO1-*mcherry-pvdA-gfp* by integrating the constitutive promoter P_{tac} linked to
213 mcherry (*att*Tn7:: P_{tac} -*mcherry*) into PAO1*pvdA-gfp* using the miniTn7 system
214 (Choi and Schweizer 2006).
215
216 ***Media and growth conditions***

217 All experiments were carried out in casamino acids medium (CAA) containing 5
218 gl^{-1} casamino acids (Merck, Switzerland), 1.18 g l^{-1} $K_2HPO_4*3H_2O$, 0.25 g l^{-1}
219 $MgSO_4*7H_2O$, and 5.96 g HEPES (all from Sigma-Aldrich). To measure the cost
220 of pyoverdine production, we grew our conditional pyoverdine mutant PAO1-
221 *pvdSi* in CAA medium supplemented with 100 μM $FeCl_3$. Under these conditions,
222 pyoverdine is not required for growth, and consequently we expect that IPTG-
223 induced pyoverdine production will induce costs, which can result in a longer lag
224 phase and/or a reduced growth rate of the bacterial culture. Thus, the cost *c* of
225 pyoverdine production at a given induction level *i* can either be measured as $c =$
226 $\lambda_0 - \lambda_i$ or $c = \mu_0 - \mu_i$, where λ_0 and μ_0 are the lag phase and the maximal growth
227 rate of non-induced PAO1-*pvdSi* cultures, whereas λ_i and μ_i represent the lag
228 phases and the maximal growth rates of induced PAO1-*pvdSi* cultures. We
229 measured the *c* for 10 induction levels (IPTG in mM: 0.1, 0.11, 0.12, 0.13, 0.14,
230 0.15, 0.175, 0.2, 0.3, 0.5) in 15-fold biological replication using multimode plate
231 readers (Tecan Infinite M200 PRO and Biotek Synergy MX). To control for
232 possible adverse effects of IPTG itself, growth in the presence of IPTG was
233 measured in both the PAO1-*pvdSi* strain (n=2) as well as in a pyoverdine knock-
234 out mutant (PAO1*ΔpvdD*) not containing an IPTG-inducible promoter (n=3; IPTG
235 in mM 0, 0.1, 0.11, 0.12, 0.13, 0.14, 0.15, 0.175, 0.2, 0.3, 0.5). Induction
236 experiments were carried out in 96-well plates, where we added approximately
237 10^5 cells from an overnight LB culture to 200 μl medium. Plates were incubated
238 in the multimode plate reader at 37°C for 24 hours. Culture growth was

239 measured as optical density (OD; absorbance at 600 nm) at 15 minute intervals.
240 Cultures were shaken for 10 minutes prior to readings. Growth curves were fitted
241 to OD trajectories from 0 to 16 hours of growth in R 3.1.1 (R Core Team 2015)
242 using functions from the 'grofit' package (Kahm et al. 2010). The Richards growth
243 model yielded the best fit for the observed growth trajectories, and was thus used
244 to estimate λ and μ values for all treatments.
245
246 In addition to OD, we also quantified the production of pyoverdine over time for
247 each IPTG induction level. Pyoverdine is a naturally fluorescent molecule, which
248 can be quantified through excitation at 400 nm and emission at 460 nm
249 (Kümmerli et al. 2009b). It has previously been shown that relative pyoverdine
250 fluorescence correlates linearly with the absolute pyoverdine content in bacterial
251 cultures (Dumas et al. 2013).
252
253 To measure the benefit of pyoverdine production, we grew PAO1-*pvdSi* in iron-
254 limited CAA medium (using 100 mg ml^{-1} human-apo transferrin to bind iron and
255 20mM $NaHCO_3$ as cofactor, both from Sigma-Aldrich, Switzerland),
256 supplemented with various amounts of purified pyoverdine (pyoverdine
257 concentration in μM: 0, 5, 10, 25, 50, 100, 200, 400; in 6-fold biological
258 replication each). Pyoverdine was extracted using the protocol described in
259 (Dumas et al. 2013), and supplemented in four time intervals (after 2, 4, 6, and 8
260 hours of growth) to mimic the continuously increasing pyoverdine concentrations

261 typically observed in growing cultures. Since PAO1-*pvdSi* was not induced with
262 IPTG in these experiments, growth was entirely dependent on the supplemented
263 pyoverdine. Accordingly, the benefit *b* of pyoverdine can be measured as $b = \mu_s$ -
264 μ_0, where μ_0 and μ_s are the maximal growth rates of the unsupplemented and
265 supplemented PAO1-*pvdSi* cultures, respectively. Measurement of growth
266 kinetics and the analysis of growth curves were carried out as described above.
267
268 To quantify cell-to-cell variation in gene expression, we used a slightly modified
269 version of the iron-limited CAA medium: 5 g Casein Hydrolysate (Merck), 0.25 g
270 $MgSO_4$*$7H_2O$ (Sigma-Aldrich), 0.9 g K_2HPO_4 (Sigma-Aldrich), and 5.96 g HEPES
271 (Sigma-Aldrich). The pH was adjusted to 7 with 5M NaOH. After autoclaving, the
272 medium was filtered through a 0.1 µm-filter in order to remove particulate iron as
273 well as background hindering the flow cytometry measurements (Cellulose
274 Nitrate Membranes, 0.1 µm, 47 mm ø, Whatman). Iron availability was adjusted
275 by addition of varying amounts of Fe(III)EDTA (Ethylenediaminetetraacetic acid
276 Iron(III)-Sodium Hydrate, Sigma-Aldrich). In order to standardize EDTA
277 concentrations across samples, iron-free EDTA (Ethylenediaminetetraacetic acid
278 disodium salt dehydrate, Sigma-Aldrich) was added to reach a total EDTA
279 concentration of 20 µM. Four iron limitation environments were tested: 0 µM, 1
280 µM, 5 µM and 20 µM Fe(III)EDTA. EDTA and Fe(III)EDTA were dissolved in
281 nanopure water, filtered through a 0.1 µm filter, and added to CAA after
282 autoclaving.

283

284 For flow cytometry and microscopy studies, the strains were streaked from a
285 frozen stock on LB agar and incubated overnight. Single colonies were picked
286 and inoculated in 5 ml LB and incubated at 37°C in an orbital shaker (220 rpm).
287 After 16 hours of incubation, the culture was diluted 1:200 in 5 ml LB and
288 regrown to the exponential phase, corresponding to an optical density of
289 approximately 0.13. To start the experiment, all strains were diluted 1:2000 to
290 reach a starting cell concentration of around 10^4 cells/ml, and inoculated in 100
291 ml CAA. Cells were cultured in 100 ml-Schott bottles in a water bath at 37°C,
292 oxygenated via stirring on a magnetic plate. The lid was removed and the bottles
293 were covered with aluminum foil to allow the cultures access to oxygen. From
294 these cultures, samples for flow cytometry and microscopy were taken.

295

296 ***Automated flow cytometry***

297 We used automated flow cytometry to monitor temporal changes in the
298 distributions of *pvdA*-reporter-associated fluorescence in cultures of *P.*
299 *aeruginosa* growing under different levels of iron limitation. Our setup, broadly
300 similar to that of (Besmer et al. 2014), enabled us to quantify the GFP fluorescent
301 signal in a time-resolved manner. To the intake port of a C6 flow cytometer (BD
302 Accuri, San Jose CA, USA), we fitted an electronically-controlled relay valve that
303 allowed switching between multiple sources. This setup permitted automated
304 time-series sampling from up to 8 cultures in parallel. GFP-signal was detected

305 using a 488 nm laser for excitation, and an emission detector fitted with a 533±30
306 nm bandpass filter. Forward- and side-scattered light produced by the 488 nm
307 laser was also quantified, and all particles associated with a forward scatter
308 signal of < 10000 fluorescence units were excluded *a priori* from further analysis
309 on the basis that they were unlikely to represent intact bacterial cells. At each
310 sampling point, the flow cytometer processed the sample at a rate of 66 µl min^{-1}
311 for two minutes, although we retained data only from the final 20 seconds of each
312 run, where the signal was most stable. Between each successive sample, the
313 line was washed with 0.2% hypochlorite and nanopure water to avoid
314 contamination and signal bleed-through. Cultures were sampled at 33-minute
315 intervals during a total period of 180 minutes. The reporter strain, PAO1*pvdA-gfp*
316 was tested in four different Fe-limitation environments (CAA supplemented with 0
317 µM, 1 µM, 5 µM and 20 µM Fe(III)EDTA, respectively). We replicated the time-
318 series experiment 8 times, where each block included the reporter strain in all
319 four environments, a blank control (i.e. CAA medium only), a negative control for
320 background GFP-fluorescence (i.e. PAO1 growing in unsupplemented CAA) and
321 two positive controls (PAO1-*gfp*, under varying levels of iron limitation). Our raw
322 flow cytometry data likely included noise – i.e. measurements from particles that
323 were not single, intact bacterial cells. Therefore, for each sample at each time
324 point, we calculated 95% contours of highest posterior density for the two-
325 dimensional space of GFP-signal versus side scatter, and we excluded from

326 further analyses any points lying outside these contours. These analyses, and all
327 others described below, were performed in R 3.1.1 (R Core Team 2015).
328
329 ***Microscopy***
330 In order to collect single-cell data on pyoverdine expression, we acquired
331 snapshots of bacterial cultures with an epifluorescence microscope. Bacteria
332 were grown in conditions identical to the flow cytometry experiments, but only
333 measured once every hour and only tested in CAA with 20 μM EDTA, without
334 addition of iron. At t=0h, cells were sampled directly from the LB medium. At 1, 2,
335 and 3 hours cells were taken from the iron-limited medium and concentrated by
336 centrifugation of 15 ml culture at 4°C, 5000 rpm, 10 minutes. Cells were kept on
337 ice until the measurement and processed within 45 minutes.
338
339 For data acquisition, 1 μl of cell suspension was spotted on a CAA 1.5% agarose
340 pad and covered with a cavity slide as described in (Bergmiller et al. 2011). We
341 used an inverted fluorescence microscope (Olympus IX81) with an X-Cite 120PV
342 fluorescence lamp (Lumen Dynamics Group Inc., Canada) and an automated
343 stage. Pictures were acquired with a cooled CCD camera (Olympus XM10) and
344 an UPLFLN 100xO2PH/1.3 phase contrast oil immersion objective (Olympus).
345 Phase contrast images were acquired with an exposure time of 20 ms,
346 fluorescence images with an exposure time of 500 ms for gfp and 800 ms for
347 mcherry. The filter for recording the GFP signal had the following parameters:

348 excitation range 450-490, emission range 500-550 nm, DM 495 nm (AHF
349 Analysentechnik, Tübingen, Germany; Article No. F46-002), the filter for mcherry:
350 excitation range 540-580, emission range 595-665, DM 585 (AHF
351 Analysentechnik, Tübingen, Germany; Article No. F46-008). Data for each type
352 of experiment were recorded within one week in order to minimize variation of
353 lamp intensity between experiments.
354
355 Growth potential of the cells was assessed by time-lapse microscopy. The
356 growth of cells was followed by acquiring phase contrast and fluorescence
357 pictures every 10 minutes for 4 hours, while cells were incubated at 37°C in a
358 temperature-controlled setup (Cube and Box incubation system, Life Imaging
359 Services, Reinach, Switzerland).
360
361 To follow microcolony growth on agarose pads, we used the same setup as
362 described above, but this time inoculating pads with a highly diluted bacterial
363 culture (dilution factor: $2.5*10^{-4}$). To induce iron limitation, we added 450 μM 2,2′-
364 bipyridin to the agarose pad. We then identified independent fields of view, which
365 contained single cells (max. 5 cells), and followed the gene expression of all cells
366 in the growing microcolony over time. Phase contrast and fluorescence pictures
367 were acquired every 15 minutes for 5 hours. We obtained time-lapse data from 5
368 fields of views and gene expression data from approximately 1000 cells in total.
369

370 Analysis of microscopy pictures was conducted with ImageJ (freely available
371 from http://rsbweb.nih.gov/ij/). First, the positions and outlines ('masks') of cells
372 within images were determined from phase contrast pictures. Cells were
373 automatically thresholded, converted into masks, and bigger cell groups were
374 split apart with the watershed filter. The position of the cell masks was stored
375 with the 'analyzing particles' command, with a size-based selection (250-Infinity
376 in pixel units). These masks were then checked manually by overlaying over the
377 phase contrast pictures, and all false positives were removed. The masks were
378 then superimposed over the fluorescence images. The background was removed
379 by subtracting a fluorescent image without cells, specific for the time point
380 measured, from the fluorescence image. If no such image was available (i.e. for
381 data for Figure 5), the average intensity of two cell-free regions was taken as
382 background. Mean gfp-values were recorded for each cell, exported and
383 analyzed in R 3.1.1. (R Core Team 2015).
384

385 **Results**

386 **Modelling reveals that division of labor can only maximize group**
387 **productivity if compound cost functions are diminishing and not linear**

388 Our mathematical model investigated conditions for which the net benefit of
389 compound production in a clonal group of cells is maximized by uniform
390 production or division of labor, respectively. Specifically, we modelled the
391 influence of the cost function (diminishing costs Fig. 1A; linear costs Fig. 1B) and

392 shareability on the net fitness ß at various proportions of producer cells in a
393 group. In the case of a diminishing cost function and low levels of compound
394 sharing, our model reveals that whether ß is maximized via specialization or
395 uniform production levels depends on the compound production level (Figure
396 1C). Specifically, low compound production maximizes the net benefit ß for
397 uniform production levels across cells because compound concentration is
398 simply too low to benefit everyone in the group. Conversely, high compound
399 production levels guarantee that still a significant amount of compounds reaches
400 nonproducing neighboring cells, despite low shareability. When considering high
401 levels of compound sharing, our model reveals that ß is always maximized
402 through specialization (Figure 1E). Thus, our model suggests that with
403 diminishing costs and high shareability we would expect bacteria to evolve
404 molecular mechanisms to restrict compound production to a fraction of the
405 individuals in a clonal group.
406
407 In contrast, when considering linear cost functions we found that specialization
408 had either a negative (Figure 1D, low shareability) or no effect on ß (Figure 1F,
409 high shareability). For linear costs, we thus expect selection to favor a uniform
410 level of compound production across cells within a clonal population. In line with
411 previous findings (Dekel and Alon 2005; Poelwijk et al. 2011), in all cases there is
412 one optimal production level that maximizes the net benefit of groups.
413

414 **Pyoverdine production entails linear costs and generates saturating**
415 **returns**

416 To estimate the cost function of pyoverdine, we induced its production in our
417 engineered conditional mutant (PAO1-*pvdSi*) across a range of IPTG
418 concentrations in iron-replete media. In this media, pyoverdine is not needed and
419 the induction of its synthesis should generate costs, possibly manifesting in an
420 extended lag phase and/or a reduced growth rate. Compatible with these
421 expectations, we found that increased levels of pyoverdine induction led to both
422 longer lag phases and lower growth rates (Figure 2A, B). These costs did not
423 manifest when a non-inducible strain was exposed to IPTG, showing that the
424 observed costs in PAO1-*pvdSi* are attributable to pyoverdine production and not
425 to potential adverse effects of IPTG (Figure S1).

426

427 When fitting statistical models to the cost data, we found that both lag phase
428 extensions and growth rate reductions scaled linearly with induced pyoverdine
429 production levels (Figure 2A, B). Interestingly, we found that a low induction of
430 PvdS actually resulted in a net benefit (i.e. negative costs) mainly in terms of
431 growth rate under iron-replete conditions. This finding is compatible with the view
432 that PvdS as a sigma factor regulates, in addition to pyoverdine production, a
433 number of other genes (Tiburzi et al. 2008), such that low PvdS expression is
434 beneficial even when pyoverdine is not needed.

435

436 Finally, we estimated the benefit function of pyoverdine by supplementing PAO1-
437 *pvdSi* with different concentrations of purified pyoverdine in iron deplete media
438 (Figure 2C). We found that benefits saturated with increasing pyoverdine
439 concentrations, indicating that above a certain level of pyoverdine availability iron
440 is either no longer the limiting resource or its uptake can no further be increased.
441

442 **Gene expression analyses indicate uniform pyoverdine production across**
443 **cells**

444 Our modeling insights combined with the discovered linear cost function for
445 pyoverdine production would predict uniform pyoverdine expression levels across
446 individuals in a clonal group. To test this hypothesis, we quantified the
447 expression of *pvdA* (encoding a pyoverdine synthesis protein) using the
448 transcriptional reporter strain PAO1 *pvdA-gfp*.
449

450 In a first analysis, we measured GFP expression of individual cells in a time-
451 resolved manner using automated flow cytometry in environments differing in iron
452 concentration. Iron availability alters the costs and benefits of pyoverdine
453 production (Kümmerli et al. 2009b), which could potentially impact both
454 individual- and group- level investment profiles. The data indeed show fine-tuned
455 adjustments of mean pyoverdine expression levels in response to iron limitation
456 and time (Figure 3A), indicating that *P. aeruginosa* adjusts pyoverdine
457 expression to match prevailing levels of iron limitation. When looking at the

458 individual-cell level, the distribution of GFP-signal intensity followed a unimodal
459 distribution, with considerable variation around the mean but no signs of
460 bimodality in *pvdA* expression across cells (Figure 3B).
461
462 We then assessed inter-individual variation in *pvdA* expression using single-cell
463 microscopy, a method that yields higher resolution of gene expression
464 differences, especially at low expression levels. In a first experiment, we
465 analyzed the *pvdA* expression of single cells grown under well-mixed conditions,
466 i.e. the same conditions used for the flow cytometry experiment. This analysis
467 confirmed our observation that *pvdA* expression followed a unimodal and not a
468 bimodal pattern at early time points of the experiment (Figure 4A). At later time
469 points we observed the emergence of a subpopulation of individuals that did not
470 express *pvdA*, but these cells neither grew nor expressed a second constitutively
471 expressed control fluorophore (mCherry; Figure 4B, C). This suggests that the
472 cells not producing pyoverdine were generally inactive, a status possibly induced
473 by the substrate shift from rich to minimal medium (van Heerden et al. 2014;
474 Kotte et al. 2014).
475
476 An implicit assumption in the above experiments is that bimodality, had it indeed
477 been observed, would have been facilitated at a mechanistic level simply by
478 intrinsic noise in expression of the genes making up the regulatory network for
479 our trait of interest. However, it could also be that bimodal expression of

480 compound production would be more clearly seen if, in addition to the intrinsic
481 gene expression noise, there was additional variability in the extracellular stimuli
482 to which the gene regulatory network is responding. Specifically, we postulated
483 that the overall range of possible pyoverdine expression levels could be widened
484 if we introduced spatial heterogeneity in local pyoverdine concentrations by
485 creating spatially structured environments. To assess this possibility, we
486 performed a second microscopy experiment, where we grew micro-colonies of
487 cells on agarose pads and followed the *pvdA* expression of individual cells over
488 time (similar to (Julou et al. 2013). This experiment also revealed a unimodal and
489 not a bimodal pyoverdine expression pattern (Figure 5).
490
491 Taken together, our flow cytometry and microscopy data are consistent with the
492 perspective that optimality in pyoverdine production in the natural environment is
493 selected for at the level of the individual cell and not the group.
494

495 **Discussion**

496 (Frank 2013) proposed that phenotypic specialization within clonal groups of
497 microbes could be common for traits entailing the secretion and sharing of
498 beneficial extra-cellular compounds between cells. Here, we formally addressed
499 this hypothesis by combining mathematical modelling with empirical experiments.
500 In line with Frank's (2013) proposition we found that high shareability of secreted
501 compounds is important for division of labor to evolve. However, in our model,

502 high shareability was neither sufficient nor the key driver of specialization.
503 Instead, our model showed that whether or not the evolution of single-cell or
504 group-level optima is favored depended on the cost function of the trait. If costs
505 scale linearly with production levels then uniform production levels maximize net
506 benefits, whereas in case of diminishing costs division of labor does (Figure 1).
507 When testing these predictions for pyoverdine, a secreted and shareable iron-
508 scavenging molecule produced by *P. aeruginosa*, we found that costs scaled
509 linearly with production levels. When probing whether division of labor is present
510 for pyoverdine production, we detected unimodal and not bimodal gene
511 expression pattern across cells. This finding is in agreement with our model and
512 suggests that linear production costs combined with the environmental conditions
513 this species faces in natural settings has selected for pyoverdine investment
514 optimization at the individual rather than the group level.
515
516 We chose pyoverdine as a model trait because it features many of the putative
517 prerequisites required for specialization to occur. At the gene regulatory level, it
518 is well established that feedback loops can generate heterogeneity in gene
519 expression (Alon 2007; Ackermann 2015). Compatible with this prerequisite,
520 pyoverdine synthesis is regulated by two interacting feedback loops. There is a
521 positive feedback loop up-regulating pyoverdine synthesis through a cell
522 membrane embedded receptor-anti-sigma-factor signaling cascade (Lamont et
523 al. 2002), and a negative feedback loop operating via Fur (ferric uptake regulator,

524 (Ochsner and Vasil 1996). At the production level, pyoverdine is synthesized via
525 NRPS, requiring the buildup of a large assembly line before compounds can be
526 produced. These initial costs (known as standing costs in economy) could
527 promote the economies of scale: a few specialists produce large quantities of a
528 product, which distributes the initial fixed costs over many units of output (Case
529 et al. 2011). Finally, we know that pyoverdine (and siderophores in general) can
530 be shared under many conditions, including laboratory (Weigert and Kümmerli
531 2017) and natural (Cordero et al. 2012; Butaitė et al. 2017) settings.
532
533 Given these prerequisites, we might ask why cells showed uniform investment
534 levels in our system, and what can we extrapolate from our findings to other
535 microbial traits? For one thing, our results show that NRPS does not
536 automatically lead to a diminishing cost function. Although perhaps
537 counterintuitive at first, our findings match recent reports that the pyoverdine
538 production machinery is metabolically inexpensive, only making up one
539 hundredth of the biomass that flows into the production of the pyoverdine
540 molecules themselves (Sexton and Schuster 2017). Although this estimate might
541 vary in response to nutrient availability (Brockhurst et al. 2008; Xavier et al. 2011;
542 Sexton and Schuster 2017), it highlights that secondary metabolite production via
543 NRPS or polyketides (Donadio et al. 2007; Caboche et al. 2007; Miethke and
544 Marahiel 2007; Weissman and Müller 2008) might often follow linear cost

patterns. Thus, diminishing cost functions might be rare even for secreted and shareable compounds.

Moreover, even in a case where costs are diminishing, our model shows that the evolution of division of labor also critically relies on high shareability of benefits. This is in line with previous models showing that the degree of compound sharing strongly influences what type of social interaction is favored by selection (Estrela et al. 2016). Although high shareability of pyoverdine (and other secreted compounds) was demonstrated in controlled experiments (e.g. s = 0.95 in well-shaken cultures; (Inglis et al. 2016), several factors could contribute to reduced sharing in natural settings, thereby compromising the efficiency of specialization (Oliveira et al. 2014). First, in certain environments including aquatic systems bacterial cells are typically dispersed and occur at low density (Whitman et al. 1998), conditions that have been shown to reduce compound sharing (Ross-Gillespie et al. 2009; Scholz and Greenberg 2015). Second, compound shareability is determined by the diffusivity of the environment (Driscoll and Pepper 2010; Allen et al. 2013; Frank 2013). High diffusivity might reduce compound sharing between neighboring individuals as compounds rapidly diffuse outside the range of cells (Kümmerli et al. 2014). Similarly, low diffusivity (e.g. in environments that are not water saturated) likely reduces shareability because compounds stay close to producers (Kümmerli et al. 2009a; Julou et al. 2013; Weigert and Kümmerli 2017). Finally, bacterial groups might often not be clonal,

567 in contrast to our model assumptions. Instead, producers could be surrounded by
568 wholly unrelated microbes that neither partake in compound production nor
569 uptake, but simply represent physical obstacles, thereby impeding efficient
570 metabolite exchange among clonemates (Inglis et al. 2016). Alternatively, the
571 community could include exploitative genotypes that use but never contribute to
572 compound production, either within the same species (Griffin et al. 2004; Cordero
573 et al. 2012) or across species (Cordero et al. 2012; Butaitė et al. 2017). In the
574 presence of exploitative genotypes, producers of siderophores were observed to
575 increase their production to high levels (Kümmerli et al. 2009b), presumably
576 leaving little room for intra-clonal division of labor to evolve.
577
578 While our model focused on the role of compound production costs and
579 shareability, there are clearly further biological and physical factors that affect the
580 evolution of division of labor. For example, cell aggregation or other factors that
581 promote group cohesion have been identified as essential elements driving the
582 selection for division of labor (Wakano et al. 2009; Rossetti et al. 2010; Ratcliff et
583 al. 2012b; Olejarz and Nowak 2014). More generally, evolutionary theory
584 suggests that division of labor is difficult to evolve in loose groups of microbes,
585 where the identity and frequency of partners can change rapidly and conflicts
586 among different genotypes might be prevalent (West et al. 2015; West and
587 Cooper 2016). This might especially hold true in fluctuating environment, where

588 conditions favoring and opposing the evolution of division of labor might quickly
589 alternate.
590
591 Despite these constraints, a number of studies showed that a genetic form of
592 division of labor can evolve in laboratory settings (Ratcliff et al. 2012a; Kim et al.
593 2016; D'Souza and Kost 2016; Dragoš et al. 2018). One issue with genetic forms
594 of division of labor is that the frequency of the two interacting partners required
595 for group optimality might not be stable. This means that in the absence of any
596 mechanism stabilizing strain frequency, one cell type could become dominant
597 and thereby lower group performance (Tasoff et al. 2015; Kallus et al. 2017;
598 Taillefumier et al. 2017). The above scenarios are different from the one
599 considered in our study, where division of labor can occur in clonal populations
600 through phenotypic specialization, and where phenotypic switching between
601 compound production and non-production could guarantee a stable proportion of
602 the two phenotypes. This form of division of labor has been reported for a
603 number of systems (infection: (Ackermann et al. 2008; Diard et al. 2013);
604 metabolism: (Flores and Herrero 2009); motility: (van Gestel et al. 2015).
605 However, unlike these examples where division of labor is explained by trade-
606 offs and task incompatibility, our theoretical model predicts that diminishing
607 production costs of a single shareable compound could drive selection of
608 phenotypic division of labor. While pyoverdine production did not allow us to test
609 this hypothesis directly, due to its linear costs, we hope that our novel hypothesis

610 will stimulate future research in the field, and result in the testing of our
611 predictions across a wider range of social traits.

Figures

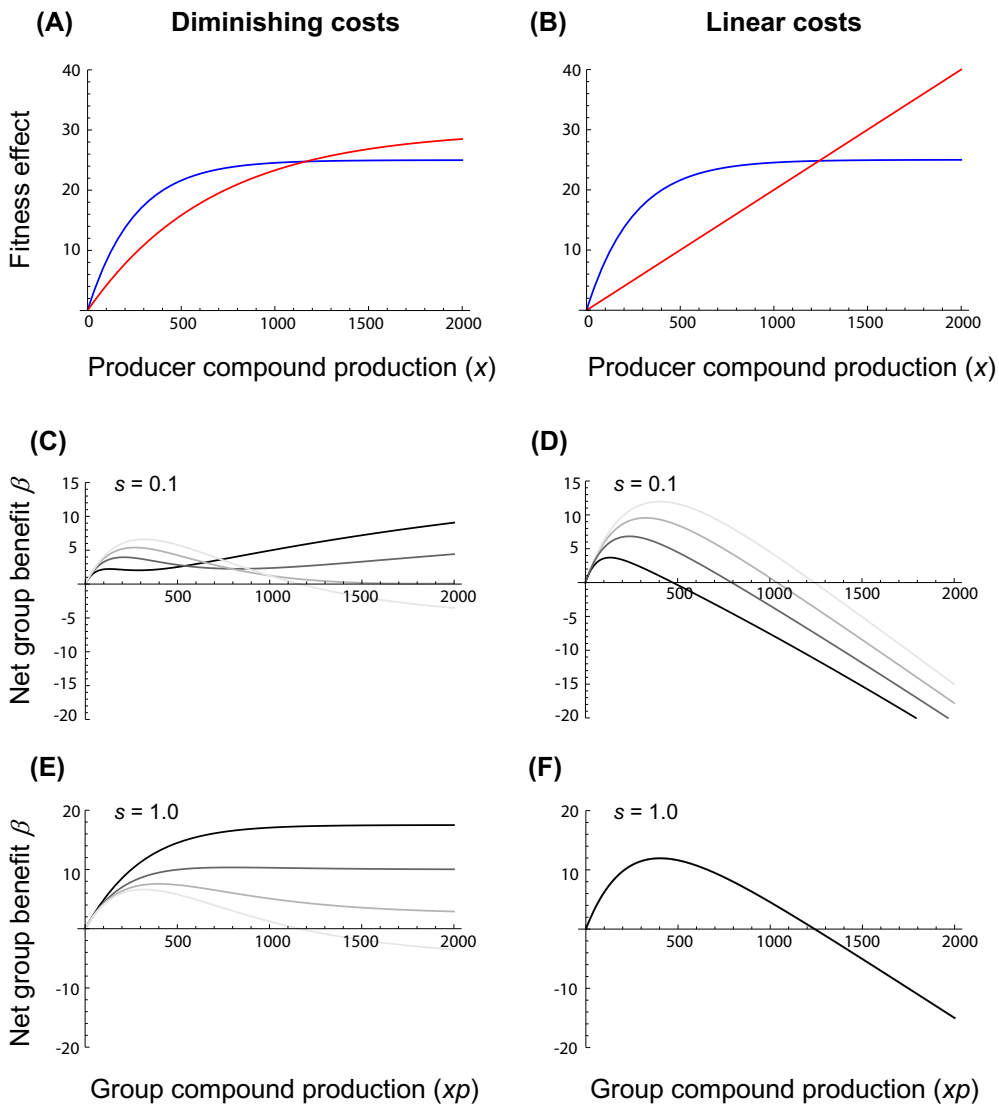

Figure 1. The net benefit to a group of bacteria producing a shared compound in relation to absolute compound production costs, shareability and the proportion of producers within the group. Panels A and B show examples of a diminishing and a linear absolute compound cost function C (red lines), respectively, in relation to a saturating gross benefit function B for producers (blue lines) assuming shareability s = 0. Panels C - F depict the resulting net benefit $\beta = B - C$ to the group as a function of group compound production (*xp*), for different values of compound shareability *s* and degrees of

production specialization p (grey shaded lines) among cells within the group: (C) diminishing costs and low shareability; (D) linear costs and low shareability; (E) diminishing costs and high shareability; (F) linear costs and high shareability. Grey shaded lines indicate scenarios for different proportions of producers, ranging from $p = 1$ (faint grey line), to $p = 0.75$ (light intermediate grey line), to $p = 0.5$ (dark intermediate grey line), to $p = 0.25$ (dark grey line). Note that maximum net group benefits equal single-cell optima for $p = 1$.

633

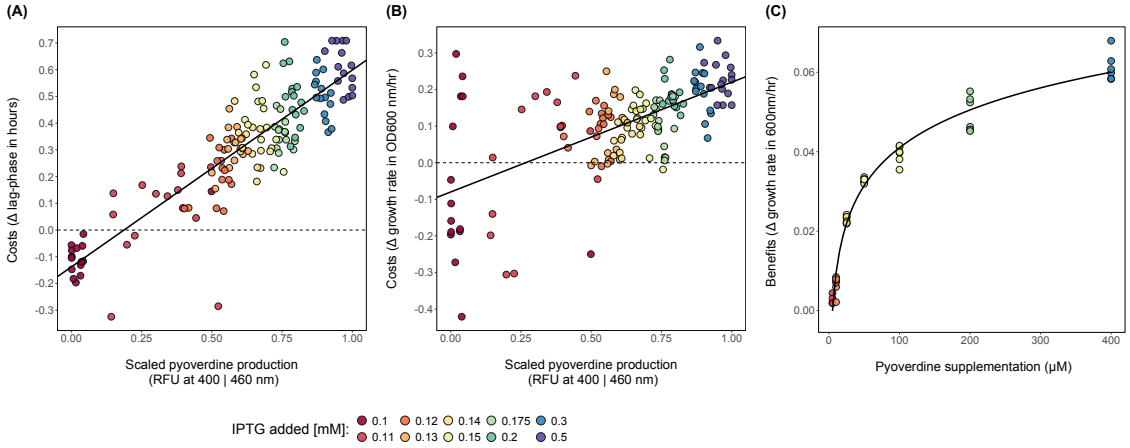

634
635

636 **Figure 2. Cost and benefit functions of pyoverdine production.** Costs were
637 measured by inducing pyoverdine production in strain PAO1-*pvdSi* by the
638 addition of increasing concentrations of IPTG under conditions where it is not
639 required for growth. (A) shows costs detectable as increased lag phase, and (B)
640 shows costs detectable as decreased growth rate. The pyoverdine peak value
641 was normalized to the pyoverdine peak at maximum induction (0.5 mM IPTG).
642 For both lag phase and growth rate costs, a linear function was the best fit, as
643 indicated in the graphs (lag-phase: $F_{1,146} = 499.5$, $R^2 = 0.772$, $p < 0.0001$; growth
644 rate: $F_{1,146} = 90.9$, $R^2 = 0.379$, $p < 0.0001$). To quantify benefits, purified
645 pyoverdine was added to cultures of non-induced PAO1-*pvdSi* under iron-
646 depleted conditions (C). We measured the increase in maximal growth rate
647 (relative to unsupplemented conditions) as a function of pyoverdine
648 supplementation. Here a logarithmic function (y = 0.01372 * log(x) -0.02216, AIC
649 = -345.4) explained more variance than either a linear (AIC = -252.8), quadratic
650 (AIC = -285.7), or an exponential (AIC = -299.1) fit. Cost and benefit functions
651 cannot directly be overlaid because the assays occurred in CAA media with
652 different iron concentrations, affecting the absolute growth rate and fitness
653 measurements (on the y-axis). However, the x-axis range is comparable for both
654 assays, assuming that 0.5 mM IPTG induces nearly maximal pyoverdine

655 production and knowing that *P. aeruginosa* maximally produces around 300 μM
656 pyoverdine in strongly iron-limited CAA over 24 hours (Dumas et al. 2013).

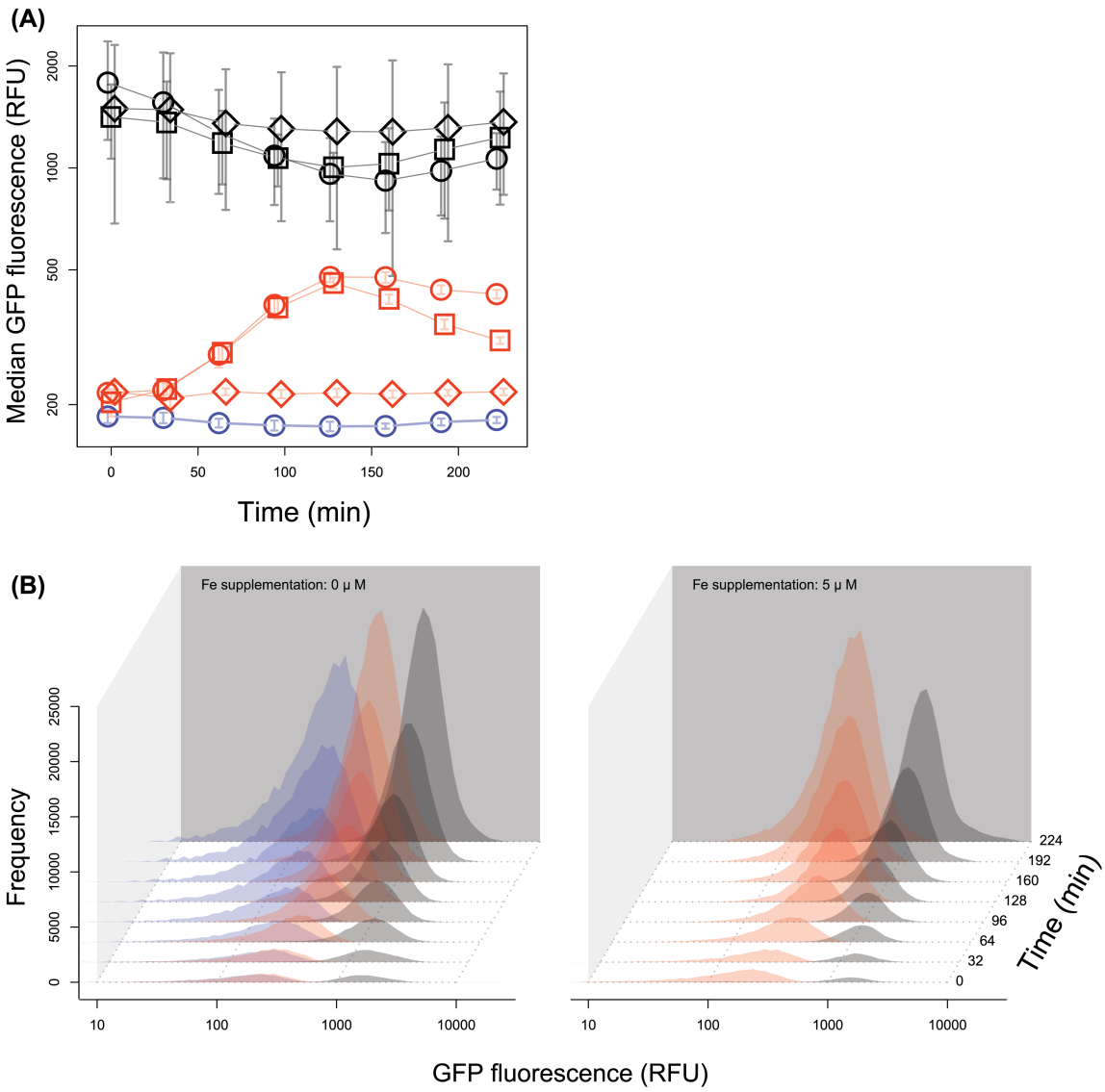

Figure 3. Tuning of pyoverdine expression in response to iron availability and time. (A) Population-level median GFP expression over time for the *pvdA-gfp* reporter (red lines) and a control strain constitutively expressing GFP (grey lines) under different iron supplementation regimes (circles = 0 μM iron added, squares = 5 μM iron added, diamonds = 20 μM iron added). The blue line depicts

667 background fluorescence signal of the wildtype PAO1 strain without reporter. (B)
668 shows the distributions of individual-level GFP expression of the *pvdA-gfp*
669 reporter (red), the constitutive *gfp* reporter (grey), and the wildtype control (blue)
670 for the 0 μM and 5 μM iron supplementation regimes, respectively. While the
671 data indicate that the absolute level of pyoverdine expression is extremely fine-
672 tuned in response to iron availability and over time, in all cases the observed
673 values are clearly unimodally distributed.
674
675
676

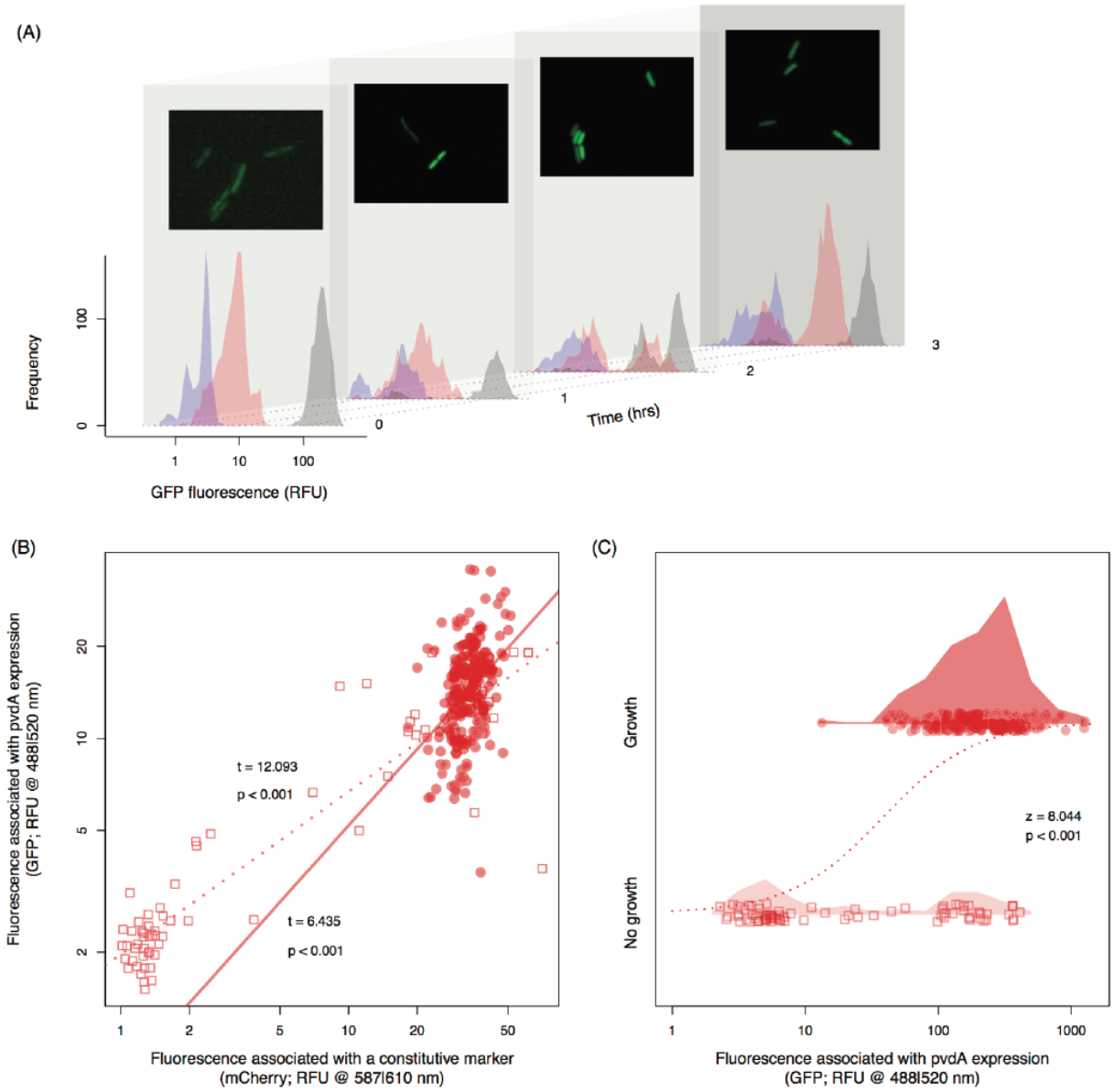

Figure 4. Microscopy confirms unimodal *pvdA* expression among growing cells. (A) Histograms show distributions of individual-level GFP expression of the *pvdA-gfp* reporter (red), the constitutive *gfp* reporter (grey), and the wildtype strain without *gfp* reporter (blue) over time. Microscopy pictures show representative snapshots of the PAO1*pvdA-gfp* strain (brightness and contrast were adjusted manually). Data reveal a significant increase in bimodality in pyoverdine expression over time (linear increase of Hartigan's *Dn*, diptest for bimodality (Maechler and Ringach 2013), for the *pvdA-gfp* reporter: t_{66} = 2.85, p

687 = 0.006, but neither for the constitutive *gfp* reporter control: t_{66} = 1.16, p = 0.249,
688 nor for the wildtype strain without *gfp*: t_{66} = -0.94, p = 0.352). However, (B)
689 fluorescence from expression of a constitutive *mcherry* control marker served as
690 a significant linear predictor of fluorescence from expression of pyoverdine
691 (*pvdA*-*gfp*) both for growing (filled circles) and non-growing cells (empty
692 squares). This suggests that pyoverdine expression levels are linked to the
693 overall cellular gene expression activity. (C) Bimodality in *pvdA*-*gfp* expression is
694 only observed among non-growing cells (squares), but was absent among
695 dividing cells (circles; ≥ 2 divisions observed within four hours) (*Dn* = 0.024, p =
696 0.485). This indicates that bimodality in pyoverdine expression at the whole
697 population level is mainly driven by bistability in the growth status of cells
698 (dashed line: significant logistic regression between a cell's pyoverdine (*pvdA*-
699 *gfp*) expression and its growth status). Shaded areas show density functions of
700 *pvdA*-*gfp* expression levels.
701
702
703
704
705
706
707

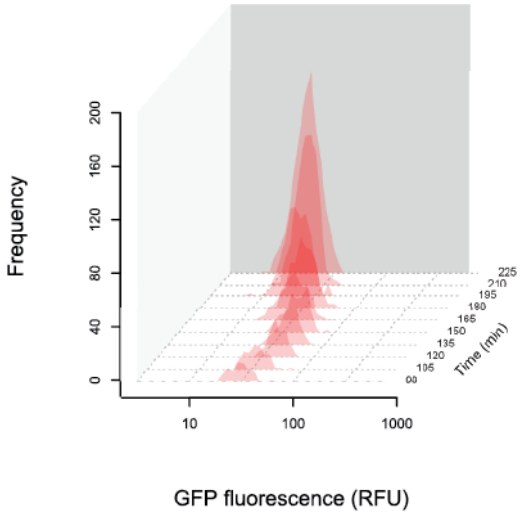

708

709 **Figure 5. The expression of *pvdA* is also unimodal when cells grow in a**
710 **spatially structured environment.** Histograms show distributions of individual-
711 level GFP expression of the *pvdA-gfp* reporter (red) over time. Cells were
712 inoculated at low density onto agarose pads and their growth and individual *pvdA*
713 expression was tracked over time using automated time-lapse microscopy. Data
714 show gene expression profiles in 30-minutes intervals, starting from 90 minutes
715 after the start of the experiment.

References

Ackermann, M. 2015. A functional perspective on phenotypic heterogeneity in microorganisms. Nature Publishing Group 13:497–508.

Ackermann, M., B. Stecher, N. E. Freed, P. Songhet, W.-D. Hardt, and M. Doebeli. 2008. Self-destructive cooperation mediated by phenotypic noise. Nature 454:987–990.

Allen, B., J. Gore, and M. A. Nowak. 2013. Spatial dilemmas of diffusible public goods. eLife 2:1–11.

Alon, U. 2007. Network motifs: theory and experimental approaches. Nat. Rev. Genet. 8:450–461.

Asfahl, K. L., and M. Schuster. 2017. Social interactions in bacterial cell–cell signaling. FEMS Microbiol Rev 41:92–107.

Bergmiller, T., R. Peña-Miller, A. Boehm, and M. Ackermann. 2011. Single-cell time-lapse analysis of depletion of the universally conserved essential protein YgjD. BMC Microbiology 11:118.

Besmer, M. D., D. G. Weissbrodt, B. E. Kratochvil, J. A. Sigrist, M. S. Weyland, and F. Hammes. 2014. The feasibility of automated online flow cytometry for in-situ monitoring of microbial dynamics in aquatic ecosystems. Front Microbiol 5:265.

Brockhurst, M. A., A. Buckling, D. Racey, and A. Gardner. 2008. Resource supply and the evolution of public-goods cooperation in bacteria. BMC Biol 6:20.

Butaitė, E., M. Baumgartner, S. Wyder, and R. Kümmerli. 2017. Siderophore cheating and cheating resistance shape competition for iron in soil and freshwater Pseudomonas communities. Nat Comms 1–12.

Caboche, S., M. Pupin, V. Leclere, A. Fontaine, P. Jacques, and G. Kucherov. 2007. NORINE: a database of nonribosomal peptides. Nucleic Acids Res 36:D326–D331.

Case, K., R. Fair, and S. M. Oster. 2011. Principles of Economics. 10 ed. Pearson Series in Economics.

Choi, K.-H., and H. P. Schweizer. 2006. Mini-Tn7 insertion in bacteria with single attTn7 sites: example *Pseudomonas aeruginosa*. Nat Protoc 1:153–161.

Cordero, O. X., L.-A. Ventouras, E. F. Delong, and M. F. Polz. 2012. Public good

dynamics drive evolution of iron acquisition strategies in natural bacterioplankton populations. Proc Natl Acad Sci U S A 109:20059–20064.

Cornforth, D. M., D. J. T. Sumpter, S. P. Brown, and Å. Brännström. 2012. Synergy and Group Size in Microbial Cooperation. Am. Nat 180:296–305.

D'Souza, G., and C. Kost. 2016. Experimental Evolution of Metabolic Dependency in Bacteria. PLoS Genet 12:e1006364.

Dekel, E., and U. Alon. 2005. Optimality and evolutionary tuning of the expression level of a protein. Nature 436:588–592.

Diard, M., V. Garcia, L. Maier, M. N. P. Remus-Emsermann, R. R. Regoes, M. Ackermann, and W.-D. Hardt. 2013. Stabilization of cooperative virulence by the expression of an avirulent phenotype. Nature 494:353–356.

Donadio, S., P. Monciardini, and M. Sosio. 2007. Polyketide synthases and nonribosomal peptide synthetases: the emerging view from bacterial genomics. Nat. Prod. Rep 24:1073.

Dragoš, A., H. Kiesewalter, M. Martin, C.-Y. Hsu, R. Hartmann, T. Wechsler, C. Eriksen, S. Brix, K. Drescher, N. Stanley-Wall, R. Kümmerli, and A. T. Kovács. 2018. Division of Labor during Biofilm Matrix Production. CURBIO 28:1903–1913.e5.

Driscoll, W. W., and J. W. Pepper. 2010. Theory for the evolution of diffusible external goods. Evolution 64:2682–2687.

Dubnau, D., and R. Losick. 2006. Bistability in bacteria. Mol Microbiol 61:564–572.

Dumas, Z., A. Ross-Gillespie, and R. Kümmerli. 2013. Switching between apparently redundant iron-uptake mechanisms benefits bacteria in changeable environments. Proc R Soc Lond [Biol] 280:20131055–20131055.

Eames, M., and T. Kortemme. 2012. Cost-benefit tradeoffs in engineered lac operons. Science 336:911–915.

Estrela, S., Morris J. J., and Kerr B. 2016. Private benefits and metabolic conflicts shape the emergence of microbial interdependencies. Environ Microbiol 18: 1415-1427.

Flores, E., and A. Herrero. 2009. Compartmentalized function through cell differentiation in filamentous cyanobacteria. Nature Rev. Microbio 8:39–50.

Foster, K. R. 2004. Diminishing returns in social evolution: the not-so-tragic commons. J. Evol. Biol. 17:1058–1072.

Frank, S. A. 2013. Evolution of Robustness and Cellular Stochasticity of Gene Expression. PLoS One 11:e1001578.

Ghysels, B., B. T. M. Dieu, S. A. Beatson, J.-P. Pirnay, U. A. Ochsner, M. L. Vasil, and P. Cornelis. 2004. FpvB, an alternative type I ferripyoverdine receptor of *Pseudomonas aeruginosa*. Microbiology (Reading, Engl.) 150:1671–1680.

Griffin, A. S., S. A. West, and A. Buckling. 2004. Cooperation and competition in pathogenic bacteria. Nature 430:1024–1027.

Inglis, R. F., J. M. Biernaskie, A. Gardner, and R. Kümmerli. 2016. Presence of a loner strain maintains cooperation and diversity in well-mixed bacterial communities. Proc R Soc Lond [Biol] 283.

Julou, T., T. Mora, L. Guillon, V. Croquette, I. J. Schalk, D. Bensimon, and N. Desprat. 2013. Cell-cell contacts confine public goods diffusion inside *Pseudomonas aeruginosa* clonal microcolonies. Proc Natl Acad Sci U S A 110:12577–12582.

Kahm, M., G. Hasenbrink, H. Lichtenberg-Fraté, J. Ludwig, and M. Kschischo. 2010. grofit : Fitting Biological Growth Curves with R. J STAT SOFTW 33.

Kallus, Y., J. H. Miller, and E. Libby. 2017. Paradoxes in leaky microbial trade. Nat Comms 8:589.

Kaneko, Y., M. Thoendel, O. Olakanmi, B. E. Britigan, and P. K. Singh. 2007. The transition metal gallium disrupts *Pseudomonas aeruginosa* iron metabolism and has antimicrobial and antibiofilm activity. J Clin Invest 117:877–888.

Kim, W., S. B. Levy, and K. R. Foster. 2016. Rapid radiation in bacteria leads to a division of labour. Nat Comms 7:10508.

Kotte, O., B. Volkmer, J. L. Radzikowski, and M. Heinemann. 2014. Phenotypic bistability in *Escherichia coli*'s central carbon metabolism. Mol Syst Bio 10:736.

Kümmerli, R., A. S. Griffin, S. A. West, A. Buckling, and F. Harrison. 2009a. Viscous medium promotes cooperation in the pathogenic bacterium *Pseudomonas aeruginosa*. Proceedings of the Royal Society B: Biological Sciences 276:3531–3538.

Kümmerli, R., K. T. Schiessl, T. Waldvogel, K. McNeill, and M. Ackermann. 2014. Habitat structure and the evolution of diffusible siderophores in bacteria. Ecol Lett 17:1536–1544.

Kümmerli, R., N. Jiricny, L. S. Clarke, S. A. West, and A. S. Griffin. 2009b. Phenotypic plasticity of a cooperative behaviour in bacteria. J Evol Biol 22:589–

598.

Lambertsen, L., C. Sternberg, and S. Molin. 2004. Mini-Tn7 transposons for site-specific tagging of bacteria with fluorescent proteins. Environ Microbiol 6:726–732.

Lamont, I. L., P. A. Beare, U. Ochsner, A. I. Vasil, and M. L. Vasil. 2002. Siderophore-mediated signaling regulates virulence factor production in Pseudomonas aeruginosa. Proc Natl Acad Sci U S A 99:7072–7077.

Maechler, M., and D. Ringach. 2013. diptest: Hartigan's dip test statistic for unimodality corrected code. R package version 0.75-5.

Miethke, M., and M. A. Marahiel. 2007. Siderophore-based iron acquisition and pathogen control. Microbiol Mol Biol Rev 71:413–451.

Ochsner, U. A., and M. L. Vasil. 1996. Gene repression by the ferric uptake regulator in Pseudomonas aeruginosa: cycle selection of iron-regulated genes. Proc Natl Acad Sci U S A 93:4409–4414.

Olejarz, J. W., and M. A. Nowak. 2014. Evolution of staying together in the context of diffusible public goods. J Theor Biol 360:1–12.

Oliveira, N. M., R. Niehus, and K. R. Foster. 2014. Evolutionary limits to cooperation in microbial communities. Proc Natl Acad Sci U S A 111:17941–17946.

Özkaya, Ö., K. B. Xavier, F. Dionisio, and R. Balbontín. 2017. Maintenance of Microbial Cooperation Mediated by Public Goods in Single- and Multiple-Trait Scenarios. Journal of Bacteriology 199:1–14.

Poelwijk, F. J., P. D. Heyning, M. G. de Vos, D. J. Kiviet, and S. J. Tans. 2011. Optimality and evolution of transcriptionally regulated gene expression. BMC Syst. Biol 5:128.

Price, M. N., A. M. Deutschbauer, J. M. Skerker, K. M. Wetmore, T. Ruths, J. S. Mar, J. V. Kuehl, W. Shao, and A. P. Arkin. 2013. Indirect and suboptimal control of gene expression is widespread in bacteria. Mol Syst Bio 9:660–660.

R Core Team, 2015. R: A language and environment for statistical computing. R Foundation for Statistical Computing, Vienna, Austria, 2012.

Ratcliff, W. C., R. F. Denison, M. Borrello, and M. Travisano. 2012a. Experimental evolution of multicellularity. Proc Natl Acad Sci U S A 109:1595–1600.

Ratcliff, W. C., R. F. Denison, M. Borrello, and M. Travisano. 2012b.

Experimental evolution of multicellularity. Proc Natl Acad Sci U S A 109:1595–1600. National Acad Sciences.

Ross-Gillespie, A., A. Gardner, A. Buckling, S. A. West, and A. S. Griffin. 2009. Density dependence and cooperation: theory and a test with bacteria. Evolution 63:2315–2325.

Rossetti, V., B. E. Schirrmeister, M. V. Bernasconi, and H. C. Bagheri. 2010. The evolutionary path to terminal differentiation and division of labor in cyanobacteria. J Theor Biol 262:23–34.

Schalk, I. J., and L. Guillon. 2013. Pyoverdine biosynthesis and secretion in Pseudomonas aeruginosa: implications for metal homeostasis. Environ Microbiol 15:1661–1673.

Scholz, R. L., and E. P. Greenberg. 2015. Sociality in *Escherichia coli*: Enterochelin Is a Private Good at Low Cell Density and Can Be Shared at High Cell Density. J Bacteriol 197:2122–2128.

Sexton, D. J., and M. Schuster. 2017. Nutrient limitation determines the fitness of cheaters in bacterial siderophore cooperation. Nat Comms 1–8.

Shachrai, I., A. Zaslaver, U. Alon, and E. Dekel. 2010. Cost of unneeded proteins in *E. coli* is reduced after several generations in exponential growth. Mol Cell 38:758–767.

Taillefumier, T., A. Posfai, Y. Meir, and N. S. Wingreen. 2017. Microbial consortia at steady supply. eLife 6:839.

Tasoff, J., M. T. Mee, and H. H. Wang. 2015. An Economic Framework of Microbial Trade. PLoS One 10:e0132907.

Tiburzi, F., F. Imperi, and P. Visca. 2008. Intracellular levels and activity of PvdS, the major iron starvation sigma factor of *Pseudomonas aeruginosa*. Mol Microbiol 67:213–227.

van Gestel, J., H. Vlamakis, and R. Kolter. 2015. From cell differentiation to cell collectives: *Bacillus subtilis* uses division of labor to migrate. PLoS Biol 13.

van Heerden, J. H., M. T. Wortel, F. J. Bruggeman, J. J. Heijnen, Y. J. M. Bollen, R. Planqué, J. Hulshof, T. G. O'Toole, S. A. Wahl, and B. Teusink. 2014. Lost in transition: start-up of glycolysis yields subpopulations of nongrowing cells. Science 343:1245114.

Veening, J.-W., W. K. Smits, and O. P. Kuipers. 2008. Bistability, Epigenetics, and Bet-Hedging in Bacteria. Annu. Rev. Microbiol. 62:193–210.

Visca, P., F. Imperi, and I. L. Lamont. 2007. Pyoverdine siderophores: from biogenesis to biosignificance. Trends Microbiol 15:22–30.

Wakano, J. Y., M. A. Nowak, and C. Hauert. 2009. Spatial dynamics of ecological public goods. Proc Natl Acad Sci U S A 106:7910–7914.

Weigert, M., and R. Kümmerli. 2017. The physical boundaries of public goods cooperation between surface-attached bacterial cells. Proceedings of the Royal Society B: Biological Sciences 284:20170631–9.

Weissman, K. J., and R. Müller. 2008. Protein–Protein Interactions in Multienzyme Megasynthetases. ChemBioChem 9:826–848.

West, S. A., and G. A. Cooper. 2016. Division of labour in microorganisms: an evolutionary perspective. Nature Rev. Microbio, doi: 10.1038/nrmicro.2016.111.

West, S. A., R. M. Fisher, A. Gardner, and E. T. Kiers. 2015. Major evolutionary transitions in individuality. Proc Natl Acad Sci U S A 112:10112–10119.

West, S. A., S. P. Diggle, A. Buckling, A. Gardner, and A. S. Griffin. 2007. The Social Lives of Microbes. Annu. Rev. Ecol. Evol. Syst. 38:53–77.

Whitman, W. B., D. C. Coleman, and W. J. Wiebe. 1998. Prokaryotes: the unseen majority. Proc Natl Acad Sci U S A 95:6578–6583.

Xavier, J. B., W. Kim, and K. R. Foster. 2011. A molecular mechanism that stabilizes cooperative secretions in *Pseudomonas aeruginosa*. Mol Microbiol 79:166–179.

Acknowledgements

We thank Frederik Hammes for support with flow cytometry. KTS, CB, and MA were supported by Eawag; KTS and MA were supported by ETH Zurich; ARG, MW and RK were supported by the Swiss National Science foundation (grant no. PP00P3-139164) and the European Research Council (grant no. 681295); KTS was supported by the Swiss National Science foundation (grant no. PP2EZP3-162260); MA was supported by the Swiss National Science foundation (grant no. 31003A_149267); MW was supported by DAAG, and DMC was supported by a University of Edinburgh studentship. The authors declare no conflict of interest.